Saltatory Propagation of Ca^{2+} Waves by Ca^{2+} Sparks

Joel Keizer,* Gregory D. Smith,# Silvina Ponce-Dawson,§ and John E. Pearson¶

*Institute of Theoretical Dynamics and Section on Neurobiology, Physiology, and Behavior, University of California, Davis, California 95616 USA; #Mathematical Research Branch, National Institute of Diabetes and Digestive and Kidney Diseases, National Institutes of Health, Bethesda, Maryland 20814 USA; §Departmento de Física and I. A. F. E., Facultad de Ciencias Exactas y Naturales, U. B. A., Cuidad Universitaria, Pabellón I, 1428 Buenos Aires, Argentina; and ¶Applied Theoretical and Computational Physics, Los Alamos National Laboratory, XCM, MS F645, Los Alamos, New Mexico 87545 USA

ABSTRACT Punctate releases of Ca^{2+}, called Ca^{2+} sparks, originate at the regular array of t-tubules in cardiac myocytes and skeletal muscle. During Ca^{2+} overload sparks serve as sites for the initiation and propagation of Ca^{2+} waves in myocytes. Computer simulations of spark-mediated waves are performed with model release sites that reproduce the adaptive Ca^{2+} release observed for the ryanodine receptor. The speed of these waves is proportional to the diffusion constant of Ca^{2+}, D, rather than $\sqrt{D}$, as is true for reaction-diffusion equations in a continuous excitable medium. A simplified "fire-diffuse-fire" model that mimics the properties of Ca^{2+}-induced Ca^{2+} release (CICR) from isolated sites is used to explain this saltatory mode of wave propagation. Saltatory and continuous wave propagation can be differentiated by the temperature and Ca^{2+} buffer dependence of wave speed.

INTRODUCTION

Fluorescence imaging of Ca^{2+} in living cells has revealed localized events referred to variously as "puffs" (Parker and Yao, 1991), "quantum emission domains" (Llinas et al., 1992), "sparks" (Cheng et al., 1993), and "elementary calcium-release units" (Horne and Meyer, 1997). These events are associated with Ca^{2+} flux into the cytosol through individual or small clusters of Ca^{2+} channels (Berridge, 1997). Ca^{2+} sparks, first characterized in cardiac myocytes (Cheng et al., 1993), also have been seen in skeletal (Schneider and Klein, 1996) and smooth muscle (Nelson et al., 1995). In myocytes sparks are associated with t-tubule structures and ryanodine receptor (RyR) Ca^{2+} channels in the sarcoplasmic reticulum (SR) (Shacklock et al., 1995; Parker et al., 1996). Ca^{2+} sparks are essential unitary events in excitation-contraction coupling (Cannell et al., 1995), and coronary defects in rats have been shown to correlate with a decreased occurrence of sparks (Gomez et al., 1997).

In myocytes sparks originate from submicron-sized sites, have a spatial extent of several microns, and a peak Ca^{2+} concentration and duration of $\sim 0.3\ \mu M$ and 100 msec, respectively (Cannell et al., 1995). In low external Ca^{2+} sparks are isolated random events, but after external Ca^{2+} is increased, sparks can serve as sites for initiation and propagation of Ca^{2+} waves. The saltatory nature of these waves (Cheng et al., 1996) and their speed ($60-80\ \mu m\ s^{-1}$) suggest that their initiation and propagation is different from other cytosolic Ca^{2+} waves, which can be described by continuous reaction-diffusion equations (Murray, 1989; Jaffe, 1993; Atri et al., 1993; Jafri and Keizer, 1995).

Here we use computer simulations to investigate how a regular array of release sites influences the propagation of Ca^{2+} waves in cardiac myocytes. We introduce a kinetic model of a release site that generalizes an earlier model of adaptation of the ryanodine receptor (Keizer and Levine, 1996) and that mimics the behavior of isolated sparks observed in cardiac myocytes. Simulations with equally spaced release sites in one spatial dimension lead to saltatory propagation of Ca^{2+} waves. We find that the saltatory wave speed is proportional to the diffusion constant of calcium, rather than its square root, as would be expected for a continuum wave. By using a simplified caricature of release sites coupled via Ca^{2+} diffusion (the "fire-diffuse-fire" model), we explore the nature of the saltatory wave. Analysis of the fire-diffuse-fire model defines the parameter range for successful wave propagation and gives a simple criterion for distinguishing saltatory and continuous propagation modes. Suggestions are made for how to distinguish saltatory and continuous propagation experimentally.

SIMULATION OF SPARKS IN MYOCYTES

We have carried out computer simulations of spark-induced waves to explore the influence of the regular array of release sites on their propagation. The simulations, which are described in the Appendix, combine Ca^{2+} diffusion with a simple kinetic model of the release site (J_{site}) and a Ca^{2+} leak (J_{leak}) and re-uptake into the SR via SERCA pumps (J_{serca}). The model release site reproduces the average rise and refractory times of a spark and includes adaptive behavior that mimics measurements on isolated RyRs in bilayers (Györke and Fill, 1993; Keizer and Levine, 1996). The simulations are deterministic, rather than stochastic, as described elsewhere (Keizer and Smith, 1998), since here we focus on wave propagation rather than initiation and termination. Fig. 1 shows a space-time (or "waterfall") plot for a typical wave (speed $v = 67\ \mu m\ s^{-1}$) initiated by a

Received for publication 14 January 1998 and in final form 6 May 1998.

Address reprint requests to Dr. Joel E. Keizer, Institute of Theoretical Dynamics, University of California–Davis, 2201 Academic Surge Bldg., One Shields Avenue, Davis, CA 95616-8618. Tel.: (530) 752-0938; Fax: (530) 752-7297; E-mail: jekeizer@ucdavis.edu.

0006-3495/98/08/595/06 $2.00

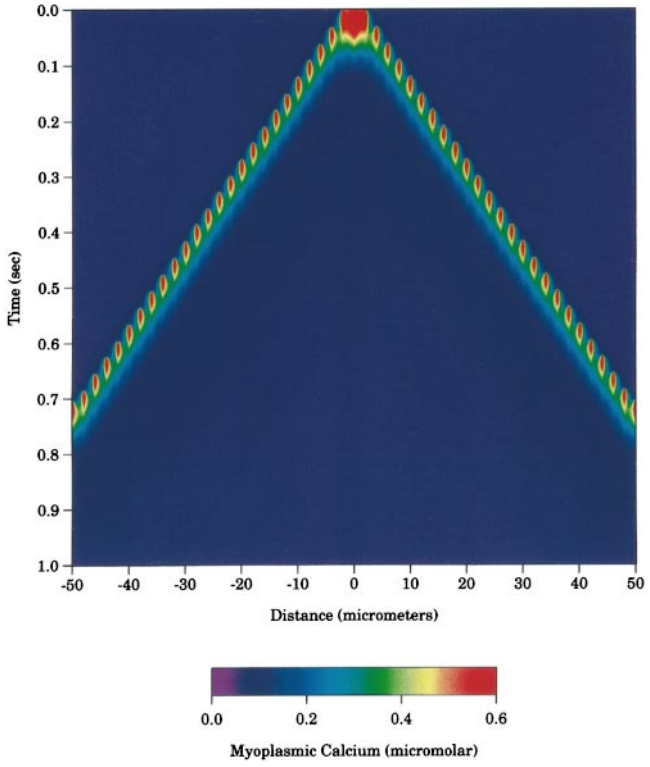

FIGURE 1 Simulated line-scan image of myoplasmic calcium ($[Ca_i^{2+}] = c$, represented by color) of a cardiac myocyte as a function of space (*horizontal axis*) and time (*vertical axis*). The reciprocal of the slope of the wave front gives the wave speed, $v = 67\ \mu m\ s^{-1}$. The simulation includes an array of 50 spatially discrete Ca^{2+} release sites, two spatially homogeneous fluxes (Ca^{2+} leak and SERCA pumps), and Ca^{2+} diffusion. See Appendix for methods.

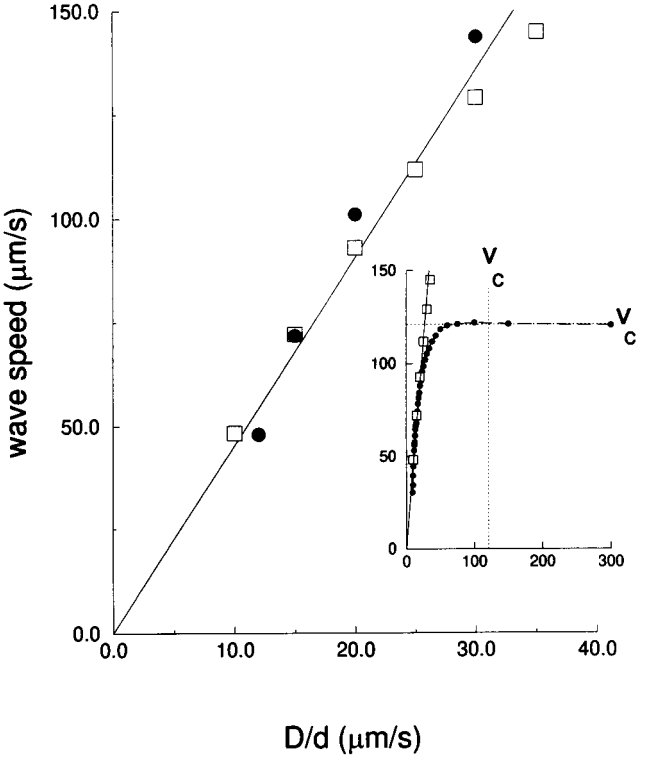

FIGURE 2 *Main graph:* Wave speed, calculated as in Fig. 1, is approximately a linear function of *D/d*. Open squares are simulations with $d = 2.0\ \mu m$ and D varied; waves do not propagate for $D < 10\ \mu m^2\ s^{-1}$. Filled circles are simulations for $D = 30\ \mu m^2\ s^{-1}$ and d varied; waves do not propagate for $d > 3.0\ \mu m$. Slope of full line is 4.5. *Inset:* Open squares, axes, and line as in main graph; filled circles for $D = 30\ \mu m^2\ s^{-1}$ and d varied with site source strength per unit length held fixed to simulate the continuum limit; the wave speed in the continuum limit, v_c, is achieved when $D/d \approx v_c$ (*dotted lines*). Other parameters as in Fig. 1.

localized increase in the myoplasmic Ca^{2+} concentration, $[Ca_i^{2+}]$, around $x = 0$ that simulates the opening of several release sites. Ca^{2+} diffuses in both directions, triggering release of additional Ca^{2+} from neighboring sites (separated by $d = 2.0\ \mu m$) via Ca^{2+}-induced Ca^{2+} release (CICR). The wave is composed of a regular sequence of sparks, evident as regions of elevated Ca^{2+} that last for ~120 ms. The shape and duration of the sparks and the wave speed, v, are comparable to that found in cardiac myocytes (Cheng et al., 1996).

If Ca^{2+} release from the isolated sites in Fig. 1 were replaced with a continuous, uniform rate of the same magnitude per unit length, the local medium would be excitable, i.e., increasing $[Ca_i^{2+}]$ above a threshold (~0.14 μM) would cause an action-potential-like spike of Ca^{2+}. An excitable medium would support a traveling wave pulse with a speed proportional to the square root of the diffusion constant (Murray, 1989; Tyson and Keener, 1988), as predicted for Ca^{2+} waves in immature *Xenopus* oocytes (Jafri and Keizer, 1995). Thus we carried out additional simulations in which either the diffusion constant of calcium, D, or the distance between release sites, d, was varied. The main graph in Fig. 2 shows that v is approximately proportional to D/d, rather than $\sqrt{D}$ (Jaffe, 1993). We find that if d is too large or D is too small, waves do not propagate.

The classical continuum limit for these simulations involves shrinking the separation between sites (d) to zero while maintaining a fixed release and re-uptake rate per unit length. Thus we have investigated the continuum limit by taking J_{site}, J_{leak}, and J_{serca} in Eq. 10 proportional to d and repeating the simulations in Fig. 1 with successively smaller values of d. A plot of the wave speed versus D/d is given in the inset to Fig. 2. The speed in the continuum limit is indicated there by v_c, and the transition to the continuum limit is seen to occur when $D/d \approx v_c$. These results make it clear that site separation significantly alters the mode of propagation of the wave.

FIRE-DIFFUSE-FIRE MODEL

To investigate why spark-mediated wave propagation differs so much from continuum propagation, we consider a caricature of the spark-mediated wave. In this simplified model release sites are located at the points $x = nd$ ($n = 0, \pm1, \pm2, \cdots$) and instantaneously release a fixed amount, σ, of Ca^{2+} when c ($=[Ca_i^{2+}]$) at a site exceeds a threshold value, c^*. After release the site becomes refractory. However, the released Ca^{2+} diffuses and may trigger another

instantaneous release (a spark) at neighboring sites. This is illustrated in Fig. 3 using overbars for the dimensionless variables: $\bar{x} = x/d$ (distance measured in terms of the site separation), $\bar{t} = tD/d^2$ (time measured in terms of the time required to diffuse between sites), and $\bar{c} = c/c^*$ (concentration measured in terms of the threshold concentration for Ca^{2+} release). We refer to this model as "fire-diffuse-fire" since a wave propagates by sequentially triggering Ca^{2+} sparks to the right (or left) by diffusion. Although the fire-diffuse-fire model is greatly simplified, it includes the essential features of fast adaptation and refractivity in that release does not occur over a sustained period and that once a site has released Ca^{2+}, it cannot release Ca^{2+} again.

The partial differential equation governing this model is

$$\partial\bar{c}/\partial\bar{t} = \partial^2\bar{c}/\partial\bar{x}^2 + \frac{1}{\alpha}\sum_{i=-\infty}^{\infty}\delta(\bar{x} - i)\delta(\bar{t} - \bar{t}_i), \qquad (1)$$

where δ is the Dirac delta function and $\bar{t}_i$ is the time that site i fires. The dimensionless parameter, $\alpha = c^*d/\sigma$, which governs the dynamics of the fire-diffuse-fire model, is the ratio of the threshold concentration for CICR (c^*) to the concentration due to release by a single site (σ/d). The value of $\bar{t}_i$ can be obtained recursively (see Eq. 6).

Thus the mean speed of a right-going wave front at site n is given by the simple formula $v_n = d/\Delta_n$ where $\Delta_n = t_n - t_{n-1}$ is the time interval between the firing of the spark at site $n - 1$ and site n. Or in terms of $\bar{\Delta}_n$,

$$v_n = D/d\bar{\Delta}_n. \qquad (2)$$

For the release event shown in Fig. 3 to trigger release from its neighboring sites, the value of $\bar{c}$ at $\bar{x} = \pm 1$ must equal 1. The first time that this occurs, if ever, is Δ_1, which can be obtained from the relationship $\bar{c} = 1$, i.e., $\alpha = \exp(-1/4\Delta_1)/\sqrt{4\pi\Delta_1}$ (see legend to Fig. 3). This can occur only when $\alpha \le 1/\sqrt{2\pi e} \approx 0.24$. This agrees with the intuition that wave initiation is favored by a low threshold (c^*), sites that are close together (d), and large releases of Ca^{2+} (σ); thus not all regular arrays of sites can initiate a wave from the firing of a spontaneous spark. For the initiation step illustrated in Fig. 3, $\bar{\Delta}_1 = 0.5$ and the initial speed is $v_1 = 2D/d$.

The speed of the wave front increases as subsequent release events contribute to the Ca^{2+} profile. The Ca^{2+} released by a site at n contributes to the overall profile of $\bar{c}$ via the formula (Murray, 1989)

$$\bar{c}(\bar{x}, \bar{t}) = \frac{1}{\sqrt{4\pi\alpha^2(\bar{t} - \bar{t}_n)}}\exp[-(\bar{x} - n)^2/4(\bar{t} - \bar{t}_n)] \qquad (3)$$

If the wave speed becomes constant (as in Fig. 1), then the interval between the firing of successive sites becomes a constant, i.e., $\bar{\Delta}_n = \bar{\Delta}$ for n large enough. In this case, by summing up the contributions in Eq. 3 over all sites it can be shown that

$$\alpha = \sum_{n=1}^{\infty}\exp(-n/4\bar{\Delta})/\sqrt{4\pi\bar{\Delta}n} = g(\bar{\Delta}), \qquad (4)$$

which defines $g(\bar{\Delta})$.

Equation 4 has a single root, $\bar{\Delta}(\alpha)$, that gives the steady wave speed

$$v = D/d\bar{\Delta}(\alpha). \qquad (5)$$

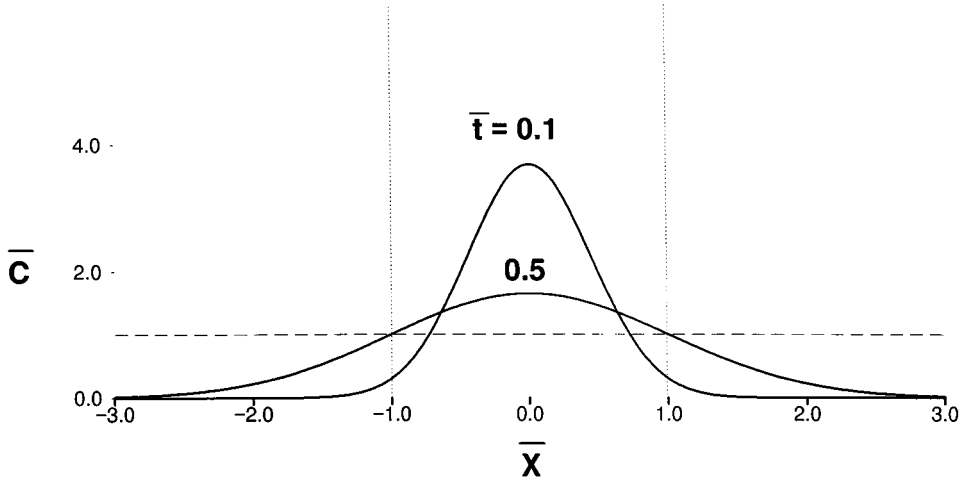

FIGURE 3 Schematic illustration of propagation for the "fire-diffuse-fire" model of spark-triggered waves (see text). Nondimensional variables $\bar{x} = x/d$, $\bar{t} = tD/d^2$, and $\bar{c} = c/c^*$ are used, giving the threshold $\bar{c}^* = 1$ shown by the dashed line. The dimensional release rate for all release sites is localized in space and time using Dirac delta function spikes, i.e., $J_{site} = \sigma\delta(x - nd)\delta(t - t_n)$, with t_n the time that the nth site fires. The nondimensional parameter for the amount of Ca^{2+} release is $\alpha = c^*d/\sigma$. The dotted vertical lines schematically show the instantaneous release of Ca^{2+} from sites $\bar{x} = \pm 1$ at $\bar{t} = 0.5$ due to a release event at $\bar{t} = 0$ from the site $\bar{x} = 0$. The Gaussian curves were calculated using the analytical formula (Murray, 1989) $\bar{c} = \exp(-\bar{x}^2/4\bar{t})/\sqrt{4\pi\alpha^2\bar{t}}$ with $\alpha = 1/\sqrt{2\pi e}$. This is the largest value of α for which release from the site at $\bar{x} = 0$ can equal the threshold $\bar{c}^* = 1$ and trigger release at its neighbors, which can be seen setting $\bar{x} = 1$ in the analytical expression for $\bar{c}$ and setting $\bar{c} = 1$.

Since Eq. 4 is independent of the diffusion constant, the wave speed is proportional to D, as found in the simulations in Fig. 2. This result also explains why the speeds of the spark-dependent waves in Figs. 1 and 2 are approximately proportional to D/d. For $\alpha \ll 1$ (i.e., large source), Eq. 4 implies that $\bar{\Delta} = 1/[4 \ln(1/\alpha)] = 1/[4 \ln(\sigma/dc^*)]$. Thus $v = 4(D/d)\ln(\sigma/dc^*)$ and the weak dependence of the wave speed on $\ln(1/d)$ would be difficult to detect. The value of $\bar{\Delta}(\alpha)$ can be obtained graphically from the plot of $g(\bar{\Delta})$ in Fig. 4.

Despite the fact that a spontaneous release event cannot initiate a wave if α is larger than ~0.24, the simultaneous release from several sites might initiate a wave with larger values of α. Indeed, since Fig. 4 shows that g can get as large as 1, it seems possible that waves could propagate with $0.24 \leq g \leq 1$. We have explored this further by applying the formula in Eq. 3 and solving iteratively for $\bar{\Delta}_n$. Indeed, when all the $\bar{t}_i$ for $-(n-1) \leq i \leq n-1$ are known, then $\bar{\Delta}_n = \bar{t}_n - \bar{t}_{n-1}$ can be obtained by solving the following equation for $\bar{t}_n$:

$$\alpha = \sum_{i=-(n-1)}^{n-1} \exp[-(n-i)^2/4(\bar{t}_n - \bar{t}_i)]/\sqrt{4\pi(\bar{t}_n - \bar{t}_i)}. \qquad (6)$$

The results of this procedure, after waiting long enough for convergence, are shown in Fig. 5. Below $\alpha = 0.512$ the interval between successive firings, $\bar{\Delta}$, converges to a constant. This value of α, however, is a critical point at which a period doubling bifurcation occurs, i.e., successive firing intervals alternate between a longer and a shorter value. This period doubling continues, leading to an apparently chaotic state for α large enough. For values of $\alpha \geq 0.535$ the chaotic attractor ceases to exist and waves do not propagate. Thus propagation failure occurs via period doubling to chaos, well below the limit of α set by Fig. 4.

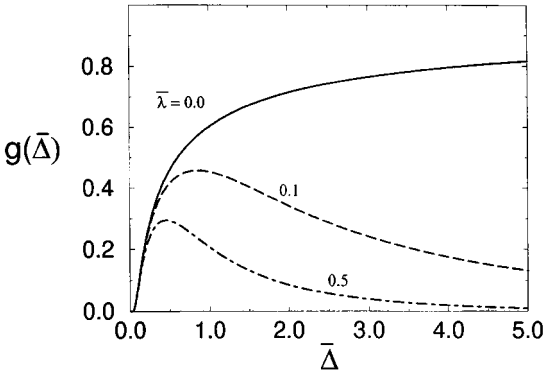

FIGURE 4 Graphical calculation of the firing interval, $\bar{\Delta}$, between adjacent sites at the front of a wave. The value of $\bar{\Delta}$ for which the function in Eq. 4, $g(\bar{\Delta})$, equals α is the firing interval for that value of α. Since $g(\bar{\Delta}) \leq 1$, waves do not propagate for $\alpha > 1$. This result is easily generalized for a spatially uniform uptake and release rate of the form $-\bar{\lambda}(\bar{c} - \bar{c}_0)$. For non-zero values of $\bar{\lambda}$ the right-hand side of Eqs. 3 and 4 are multiplied by $\exp(-\bar{\lambda}\bar{t})$ and $\exp(-\bar{\lambda}\bar{\Delta})$, respectively. If $\bar{c}_0 > 0$, then the left-hand side of Eq. 4 must also be multiplied by $1 - (\bar{c}_0/\bar{c}^*)$. The resulting sum is plotted for $\bar{\lambda} = 0.1$ and 0.5.

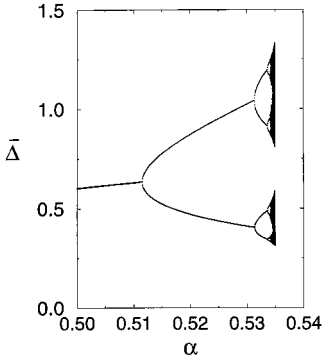

FIGURE 5 The "firing interval", i.e., the time interval between adjacent sparks at the front of the wave, is obtained by successively calculating $\bar{\Delta}_n$ for $n = 1, 2, \ldots$ using Eq. 3 and the criterion $\bar{c}(n, \bar{t}_n) = 1$ for a range of values of α. The wave was initiated by simultaneously firing all the sites for $-15 \leq n \leq 15$. A period doubling cascade begins at $\alpha \approx 0.512$, which terminates in a chaotic state at $\alpha \approx 0.535$, beyond which waves do not propagate.

The period doubling cascade produces a rhythmic alteration in the progress of the wave front. For $\alpha < 0.512$ the time interval between Ca^{2+} release at the frontmost site (n) and the next site ($n + 1$) is fixed. Using Eq. 5, this implies that the wave front propagates at a fixed speed. This steady propagation changes at the first period doubling bifurcation, where the time interval between release at site n and $n + 1$ becomes slightly longer than the interval between sites $n + 1$ and $n + 2$; thus the speed of the front alternates between a slower and faster value, giving a slightly jerky appearance to the front. At the second period doubling bifurcation the wave propagation is more complex, with four alternating speeds. This continues with propagation becoming increasingly more complex at each period double bifurcation until finally propagation failure occurs at the chaotic state. Although these specific dynamical features are not seen in simulations with a two-dimensional array of sites (not shown), a rich variety of complex dynamics are still observed near the propagation failure limit.

Similar results are obtained if we introduce a linear, spatially uniform uptake and release of Ca^{2+} from the SR with rate constant λ, as described in the legend to Fig. 4. The plots of $g(\bar{\Delta})$ for $\bar{\lambda} = 0.1$ and 0.5, however, now have a maximum. Thus for $\bar{\lambda} > 0$, the solution to Eq. 4 has two roots. The larger value of $\bar{\Delta}$ corresponds to the intersection on the declining branch of the curve in Fig. 4 and a wave that is slower and unstable.

DISCUSSION

The saltatory nature of Ca^{2+} wave propagation in cardiac myocytes has been revealed only recently using high-speed, high-resolution line scan images (Cheng et al., 1996). The correlation between the underlying Ca^{2+} sparks and the regular array of t-tubule structures in these images provided the motivation for the one-dimensional simulations that we report here. By using a model of a release site based on the

kinetics of ryanodine receptors (Smith, 1996; Keizer and Smith, 1998) we have found that these waves propagate with a speed that is proportional to the diffusion coefficient of Ca^{2+}, rather than its square root as prediction by conventional reaction-diffusion equations (Jaffe, 1993; Jafri and Keizer, 1995). Our results in Fig. 2 (*inset*) illustrate the connection between these two extreme types of wave propagation, saltatory and continuous. In the saltatory case the value of $[Ca_i^{2+}]$ at the wave front is dominated by release from a single site (c.f. Fig. 1). For continuous propagation, release is distributed continuously in space and many sites at the front release Ca^{2+} simultaneously.

The "fire-diffuse-fire" model, which we have introduced to help explain saltatory propagation, is a simplified model of CICR by release sites with a refractory state. In this model a site releases Ca^{2+} instantaneously ("fires") when the value of $[Ca_i^{2+}]$ at the site exceeds a threshold value. To mimic a long-lasting refractory state, once a site has released Ca^{2+}, it can no longer fire again. To mimic the regular array of t-tubules in myocytes, the release sites are located with a fixed separation, d, and Ca^{2+} released at one site diffuses continuously with an "effective" diffusion constant, D, due to the presence of myoplasmic buffers. In this model the speed of the wave front is determined by the time it takes Ca^{2+} released by the site at the front to diffuse to the next active site and raise the value of $[Ca_i^{2+}]$ there to the threshold (c.f. Eq. 2). In contrast to the kinetic model, the fire-diffuse-fire model leads to analytical expressions for the wave shape and the wave speed, and therein lies its value. Indeed, the simple result illustrated graphically in Fig. 3 makes it clear that the wave speed is proportional to the diffusion constant since the time to diffuse between release sites (d^2/D) is inversely proportional to the diffusion constant. The model also suggests that propagation failure of saltatory waves may be quite complex.

The simplifying assumption of instantaneous release of Ca^{2+} in the fire-diffuse-fire model is not responsible for the saltatory nature of the waves. Indeed, the simulations with the kinetic model in Fig. 1 do not make this assumption and yet exhibit saltatory propagation. We have investigated this further using a generalization of the fire-diffuse-fire model in which release is not instantaneous (J. Pearson, J. Keizer, and S. Ponce-Dawson, unpublished observations). We find that a key dimensionless number is $D\tau/d^2$ where τ is the mean time that a site is open and d^2/D is the intersite diffusion time. When $D\tau/d^2 \ll 1$, propagation is saltatory and the wave speed is proportional to D, as we have shown. In the saltatory limit, propagation consists of isolated bursts of Ca^{2+} that occur as each consecutive site fires. When $D\tau/d^2 \gg 1$, propagation is continuous, the velocity is proportional to $\sqrt{D}$, and many sites are releasing Ca^{2+} simultaneously.

This analysis explains the transition from saltatory to continuous propagation shown in the inset to Fig. 2. According to the Luther equation the continuum wave speed should be given by the expression $v_c = \sqrt{D/\tau}$ (Jaffe, 1993). In terms of v_c, the dimensionless parameter $D\tau/d^2$ can, therefore, be rewritten as $(D/dv_c)^2$. Thus the analysis in the previous paragraph predicts that the transition between saltatory and continuous propagation occurs when $D/d \approx v_c$. Moreover, due to the second-power dependence of the ratio $(D/dv_c)^2$, the transition should be relatively sharp. This agrees with both the location and sharpness of the transition for the simulations plotted in the inset of Fig. 2. It is easy to evaluate the ratio $D\tau/d^2$ using experimental data for cardiac myocytes ($D = 30\ \mu m^2\ s^{-1}$, $\tau = 14$ ms, and $d = 2.0\ \mu m$; Smith et al., 1998). This gives $D\tau/d^2 = 0.1$, which is well into the saltatory regime. This prediction is compatible with the punctate images of the wave front that result from enhancement of Ca^{2+} waves in myocytes (Cheng et al., 1996).

The fire-diffuse-fire model suggests experimental tests that distinguish saltatory from continuously propagating Ca^{2+} waves. The linear dependence of v on D should show up in the dependence of wave speed on temperature. Indeed, from the Arrhenius equation, $D = D_o \exp(-E_a/RT)$, where E_a is the activation energy for diffusion. Generally, this is much smaller than the activation energy for the biochemical processes that determine the activation energy associated with τ. This implies that the speed of a saltatory wave, which is proportional to D/d, should be less sensitive to changes in temperature than predicted by the Luther equation, which gives $v_c = \sqrt{D/\tau}$. Using exogenous Ca^{2+} buffers it also should be possible to manipulate the diffusion constant of Ca^{2+} (Wagner and Keizer, 1994), which would alter the wave speed differently for saltatory and continuous propagation.

Several predictions of the fire-diffuse-fire model are in agreement with published observations of waves in cardiac myocytes. Thus the saltatory structure of the waves in the fire-diffuse-fire model, when displayed as in Fig. 1, are similar to the images obtained from line-scan data in myocytes (Cheng et al., 1996). The fact that there is a maximum value for $\alpha = c^*d/\sigma$ above which waves do not initiate is compatible with the fact that Ca^{2+} overloading of myocytes is a prerequisite for waves, i.e., the source strength, σ, must be sufficiently large (Cheng et al., 1996). The dependence of the wave speed on α (c.f. Fig. 5) may help explain irregularities in the speed of the wave front as it moves across a myocyte (Cheng et al., 1996) since both d and store content (σ) may vary somewhat within a cell. Finally, the observation that wave propagation is irregular just before propagation failure may be related to the onset of chaos that is seen in the fire-diffuse-fire model (Cheng et al., 1996).

What do these results tell us about the physiological role for saltatory propagation of Ca^{2+} waves in cells? In fact, the saltatory Ca^{2+} waves observed in cardiac myocytes and the immature *Xenopus* oocyte (Callamaras et al., 1998) both occur only under extreme physiological conditions. Therefore, it is possible that the punctate arrangement of release sites in these cells actually functions to *inhibit* Ca^{2+} waves by guaranteeing propagation failure under normal physiological conditions. This would contrast with saltatory propagation of action potentials in myelinated nerve, where the nodes of Ranvier are analogous to release sites (Fitzhugh, 1962). In this case, the saltatory wave speed has been reported to exceed that for the continuum limit. This differ-

ence from what we find for the Ca^{2+} wave in myocytes (c.f. Fig. 2, *inset*) is probably due to the finite size of the nodes and may reflect the different physiological roles of CICR and action potentials in the two cell types. On one hand, in muscle Ca^{2+} release is believed to act locally and, thus, failure of a propagating Ca^{2+} signal would be appropriate physiologically. In myelinated nerve, on the other hand, action potentials are transmitted to distant cells and nodes are utilized to reinforce their propagation.

APPENDIX: SIMULATION METHODS

The simulations in Figs. 1 and 2 were carried out on an IBM RS6000 workstation. The simulation utilizes an array of 50 spatially discrete Ca^{2+} release sites, two spatially homogeneous fluxes (Ca^{2+} leak and SERCA pumps), and Ca^{2+} diffusion. Each release site is implemented using a two-state model ($N \leftrightarrow R$) where the nonrefractory state, N, consists of two open and two closed states that rapidly equilibrate and the refractory state, R, consists of two equilibrated closed states (Keizer and Levine, 1996; Smith, 1996; Keizer and Smith, 1998). The fractional release rate of each site is

$$f_O = f_N \frac{c^8}{K_e K_a}\left(1 + \frac{c_d^4}{K_b}\right)/B \tag{7}$$

with

$$B = 1 + \frac{c^4}{K_e}\left(1 + \frac{c^4}{K_a}\left(1 + \frac{c_d^4}{K_b}\right)\right) \tag{8}$$

and the dynamics of inactivation and recovery are governed by

$$df_N/dt = -\rho_0 f_N + \rho_1(1 - f_N) \tag{9}$$

where $\rho_0 = [(k_c^- c^8 c_d^4/K_e K_a K_b) + (k_d^+ c^8/K_e)]/B$ and $\rho_1 = K_f(k_c^+ c^4 + k_d^-)/(K_f + c^4)$.

The release sites are 0.1 μm wide, centered at $x = nd$ (integer n, $-25 \le n \le 25$), and the flux per site is $J_{site} = v_1 f_O(c_{sr} - c)$ where $c_{sr} = (c_0 - c)/c_1$ relates SR and myoplasmic Ca^{2+}. The release sites are coupled via Ca^{2+} diffusion, and we solved the equation

$$\partial c/\partial t = D\partial^2 c/\partial x^2 + J_{site} + J_{leak} - J_{serca} \tag{10}$$

using a Crank-Nicolson method (periodic boundary conditions, $\Delta t = 0.001$ ms, $\Delta x = 0.1$ μm) where $J_{leak} = v_2(c_{sr} - c)$ and $J_{serca} = v_3 c^4/(k_3^4 + c^4)$. The sites are equilibrated initially with basal $[Ca_i^{2+}]$ ($c = 0.061$ μM) and the wave is triggered by setting $c = 0.50$ μM on the interval -3 μm $\le x \le$ 3 μm.

The parameters used in the simulations, unless otherwise indicated, are the following: site separation $d = 2.0$ μm; Ca^{2+} diffusion constant $D = 30$ $\mu m^2\ s^{-1}$ (reduced to account for Ca^{2+} binding to buffers); Ca^{2+} binding constants $K_a = 0.0192$, $K_b = 0.257$, $K_c = 20$, $K_d = 0.247$, $K_e = 5$, $K_f = 60$ (μM^4); rate constants $k_d^+ = 5000$, $k_c^+ = 3.33$ ($\mu M^{-4}\ s^{-1}$); $k_d^- = 1.24$, $k_c^- = 66.7$ (s^{-1}); elevated "domain" Ca^{2+} when the site is open $c_d = 10$ μM; maximum Ca^{2+} fluxes $v_1 = 200$, $v_2 = 0.01$, $v_3 = 10$ ($\mu M\ s^{-1}$); pump affinity $k_3 = 0.184$ μM; total free Ca^{2+} concentration $c_0 = 1.2$ μM; SR-to-myoplasm volume ratio $c_1 = 0.1$.

The authors thank J. Tyson, L. Jaffe, J. Rinzel, A. Sherman, W. Horsthemke, D. Sigeti, M. Mineev, and R. Webster for useful conversations regarding this work, and R. Miura for a careful reading of the manuscript.

This work was supported National Science Foundation Grant BIR 9214381 and National Institutes of Health Grant R01 RR10081 (to J.K.), the Agricultural Experiment Station at University of California–Davis, and an Intramural Research Training Assistantship Fellowship (to G.S.).

REFERENCES

Atri, A., J. Admunson, D. Clapham, and J. Sneyd. 1993. A single pool model for intracellular calcium oscillations and waves in the *Xenopus laevis* oocyte. *Biophys. J.* 65:1727–1739.

Berridge, M. J. 1997. Elementary and global aspects of calcium signaling. *J. Physiol. (Lond.).* 499:291–306.

Callamaras, N., J. S. Marchant, X.-P. Sun, and I. Parker. 1998. Activation and coordination of $InsP_3$-mediated elementary Ca^{2+} events during global Ca^{2+} signals in *Xenopus* oocytes. *J. Physiol. (Lond.).* 509:81–91.

Cannell, M. B., H. Cheng, and W. J. Lederer. 1995. The control of calcium release in heart muscle. *Science.* 268:1045–1049.

Cheng, H., M. R. Lederer, W. J. Lederer, and M. B. Cannell. 1996. Calcium sparks and $[Ca_i^{2+}]$ waves in cardiac myocytes. *Am. J. Physiol.* 270:C148–C159.

Cheng, H., W. J. Lederer, and M. B. Cannell. 1993. Calcium sparks—elementary events underlying excitation-contraction coupling in heart muscle. *Science.* 262:740–744.

Fitzhugh, R. 1962. Calculation of impulse initiation and saltatory conduction in a myelinated nerve fiber. *Biophys. J.* 2:11–27.

Gomez, A. M., H. H. Valdivia, H. Cheng, M. R. Lederer, L. F. Santana, M. B. Cannell, S. A. McCune, R. A. Altschuld, and W. J. Lederer. 1997. Defective excitation-contraction coupling in experimental cardiac hypertrophy and heart failure. *Science.* 276:800–806.

Györke, S., and M. Fill. 1993. Ryanodine receptor adaptation—control mechanism of Ca^{2+}-induced Ca^{2+} release in heart. *Science.* 260: 807–809.

Horne, J. H., and T. Meyer. 1997. Elementary calcium-release units induced by inositol trisphosphate. *Science.* 276:1690–1693.

Jaffe, L. 1993. Classes and mechanisms of calcium waves. *Cell Calcium.* 14:736–745.

Jafri, S., and J. Keizer. 1995. On the roles of Ca^{2+} diffusion, Ca^{2+} buffers, and the endoplasmic reticulum in IP_3-induced Ca^{2+} waves. *Biophys. J.* 69:2139–2153.

Keizer, J., and L. Levine. 1996. Ryanodine receptor adaptation and Ca^{2+}-induced Ca^{2+} release-dependent Ca^{2+} oscillations. *Biophys. J.* 71: 3477–3487.

Keizer, J., and G. D. Smith. 1998. Spark-to-wave transition: saltatory transmission of calcium waves in cardiac myocytes. *Biophys. Chem.*, in press.

Llinas, R., M. Sugimori, and R. B. Silver. 1992. Microdomains of high calcium concentration in a presynaptic terminal. *Science.* 256:677–679.

Murray, J. D. 1989. Mathematical Biology. Springer-Verlag, Berlin. 232–238, 277–286, 328–335.

Nelson, M. T., H. Cheng, M. Rubart, L. F. Santana, A. D. Bonev, H. J. Knot, and W. J. Lederer. 1995. Relaxation of arterial smooth muscle by calcium sparks. *Science.* 270:633.

Parker, I., and Y. Yao. 1991. Regenerative release of calcium from functionally discrete subcellular stores by inositol trisphosphate. *Proc. R. Soc. Lond. B.* 246:269–275.

Parker, I., W.-J. Zang, and W. G. Wier. 1996. Ca^{2+} sparks involving multiple Ca^{2+} release sites along Z-lines in rat heart cells. *J. Physiol. (Lond.).* 497:31–38.

Schneider, M. F., and M. G. Klein. 1996. Sarcomeric calcium sparks activated by fiber depolarization and by cytosolic Ca^{2+} in skeletal muscle. *Cell Calcium.* 20:123–128.

Shacklock, P. S., W. G. Wier, and C. W. Balke. 1995. Local Ca^{2+} transients (Ca^{2+} sparks) originate at transverse tubules in rat heart cells. *J. Physiol. (Lond.).* 487:601–608.

Smith, G. D. 1996. Doctoral thesis, University of California, Davis.

Smith, G. D., J. E. Keizer, M. D. Stern, W. J. Lederer, and H. Cheng. 1998. A simple numerical model of calcium spark formation and detection in cardiac myocytes. *Biophys. J.* 75:15–32.

Tyson, J., and J. P. Keener. 1988. Singular perturbation theory of travelling waves in excitable media. *Physica D.* 32:327–351.

Wagner, J., and J. Keizer. 1994. Effects of rapid buffers on Ca^{2+} diffusion and Ca^{2+} oscillations. *Biophys. J.* 67:447–456.